

Semileptonic six fermion processes at future e^+e^- colliders: signal and irreducible background for top and WWZ physics.¹

Elena Accomando, Alessandro Ballestrero and Marco Pizzio

I.N.F.N., Sezione di Torino, Italy

and

Dipartimento di Fisica Teorica, Università di Torino, Italy

v. Giuria 1, 10125 Torino, Italy.

Abstract

We compute several total and differential cross sections relevant to top and WWZ physics at future e^+e^- colliders taking into account the full set of Feynman diagrams for six fermion final states. We also include in our calculations initial state radiation and beamstrahlung effects, and the most important QCD corrections in an approximate (naive) form. We compare such a complete approach with *production* \times *decay* approximation and we suggest that in many physical studies the former is needed.

¹ Work supported in part by Ministero dell' Università e della Ricerca Scientifica.

1 Introduction

Since the advent of helicity amplitude methods [1] [2] [3], various processes with many particles and a great number of tree level Feynman diagrams have been computed successfully. These processes become more and more important at high energies for present and future accelerators. In e^+e^- physics, with the advent of LEP2, WW and Higgs studies are now being performed with the help of the electroweak dedicated four fermion codes [4] [5] [7] [8]. Most of them compute the amplitudes taking into full account all Feynman diagrams and some can provide cross sections for all possible 4 fermion processes. Previous computations relied on calculating the differential cross sections for $e^+e^- \rightarrow W^+W^-$, $e^+e^- \rightarrow HZ$ or $e^+e^- \rightarrow ZZ$ and folding them with the differential branching for the successive decay of W's, Z's and H. With such a method it has been possible to compute strong and electroweak corrections to production and decay. However with such *production* \times *decay* approximation, one is of course neglecting the contributions due to many Feynman diagrams as well as the off-shellness of signal diagrams. Spin correlation effects are also disregarded, as one sums over all possible final helicities of the intermediate state W's and Z's, and then computes their decay as unpolarized particles. Only with the complete calculations it is possible to determine the magnitude of such approximations. Various phenomenological analyses [9] [10] have shown that, even if *production* \times *decay* may often be reliable for fully extrapolated total cross sections, it is certainly not a good approximation when experimental cuts are implemented and when one is interested in differential cross sections.

When future e^+e^- colliders will come into operation, states with even more final state particles will become of the utmost interest. In particular all physics regarding top studies and three vector boson production will be concerned with six fermion final states. For such a reason we compute in this paper all semileptonic six fermion processes with four final quarks and compare in detail the full calculation versus *production* \times *decay* approximations for some cross sections and distributions of interest. We consider for the time being only the case in which one has no Higgs which can decay into two W's. Of course if that would not be the case, Higgs production itself would end up in a six fermion process. Top and Higgs physics have already been analyzed in this respect within a four particles ($b\bar{b}W^+W^-$) final state approximation [11]. Other groups are at present working on six fermion final state physics [12][13]. In particular in ref.[12] the processes $e^+e^- \rightarrow \mu^+\mu^-\tau^-\bar{\nu}_\tau u\bar{d}$ and $e^+e^- \rightarrow \mu^+\mu^-e^-\bar{\nu}_e u\bar{d}$ have been computed with the inclusion of an intermediate Higgs contributions and these reactions have been used to discuss the relevance of six fermion full calculations for Higgs physics. Other computations [13] have been performed on $e^+e^- \rightarrow b\bar{b}u\bar{d}\mu^-\bar{\nu}_\mu$ which is instead of major interest to top physics in the continuum.

The plan of the paper is the following: in section 2 we analyze some general properties of all possible six fermion processes for e^+e^- colliders, in section 3 we give some details of the calculation, in section 4 we present our results for top physics, while section 5 will cover WWZ physics. Some considerations and outlooks are given in the conclusions.

2 $e^+e^- \rightarrow \text{sixfermion processes}$

All processes $e^+e^- \rightarrow \text{sixfermions}$ can be divided according to their final states. As for four fermion final states, we can identify Charged Currents (CC), Neutral Currents (NC) and Mixed processes (MIX) [14][7] [5]. The final states for six fermion processes can in fact be deduced from the corresponding ones for four fermions, adding to them a particle antiparticle pair.

For four fermions the convention is to call CC those processes in which the final particles can form two W's and not two Z's (e. g. $\mu\bar{\nu}u\bar{d}$), NC those in which they form two Z's, but cannot form two W's (e. g. $u\bar{u}\mu^+\mu^-$) and MIX those in which they can form both (e. g. $u\bar{u}d\bar{d}$).

Of course this implies that in every single diagram of CC processes there is at least one charged current, but it does not exclude neutral currents. Also for NC one can have charged currents (as it is the case for $\nu_e\bar{\nu}_e b\bar{b}$) together with neutral ones.

We will from now on call CC the six fermion processes in which the final particles can form two W's and a Z but not three Z's (e. g. $\mu\bar{\nu}u\bar{d}e^+e^-$), NC those in which three Z's and not two W's and a Z can be formed (e. g. $u\bar{u}\mu^+\mu^-e^+e^-$), MIX those in which both can be formed (e. g. $u\bar{u}d\bar{d}e^+e^-$).

Six fermion CC processes are of particular interest because they are related to top, WWZ and Higgs physics. If we consider for instance a final state like $b\bar{b}\mu\bar{\nu}_\mu u\bar{d}$, this may be produced by the decay of WWZ or come from two W's and two b's, which in turn may descend from two tops. WWZ intermediate state may be due to Higgs Z production with an Higgs decaying into two W's. Final states like $\nu_e\bar{\nu}_e\mu\bar{\nu}_\mu u\bar{d}$ may be produced by the $WW \rightarrow H$ fusion diagram (which dominates upon Higgs strahlung at energies $\gtrsim 500$ GeV) and successive decay of the Higgs as above. Of course the various channels are not separated in the reality, and many more diagrams (irreducible background) contribute to such processes. They can be distinguished only for their different contribution to various zones of the phase space and can therefore be disentangled by applying experimental cuts. In order to study such cuts, and to evaluate the magnitude of the various contributions after they have been applied, it is fundamental to use the full calculation. This is precisely what we do for CC semileptonic processes, i. e. for the case in which two of the particles which can reconstruct a W are a lepton and a neutrino. With such a prescription, we are excluding all processes with four quarks reconstructing two W's, as for instance $\mu^+\mu^-u\bar{d}\bar{c}s$ or the fully hadronic $b\bar{b}u\bar{d}\bar{c}s$. It would have been straightforward to include in our analysis such processes, but it is meaningless to consider them without NC and MIX events. When four quarks are present in the final state, different flavors cannot be experimentally recognized (apart from b-tagging), so that $\mu^+\mu^-u\bar{d}\bar{c}s$ (CC) cannot be distinguished from $\mu^+\mu^-u\bar{d}\bar{u}d$ (MIX) or $\mu^+\mu^-u\bar{u}s\bar{s}$ (NC). This consideration shows that on one side considering non semileptonic processes makes computations much longer if not harder, on the other that the semileptonic events will be much cleaner and easy to study also from an experimental point of view.

Keeping in mind that for the hadronic case all CC, NC, MIX processes have to be considered, let us briefly discuss pure NC events. In principle they are of course relevant as they can be produced by three Z's or from two Z's and a separate pair. So it seems

that their main interest within the Standard Model corresponds to Higgs strahlung or ZZ fusion with successive Higgs decay in two Z's. These events are depressed with respect to the corresponding Higgs \rightarrow WW ones by the different branching ratios and for the higher cross sections of $e^+e^- \rightarrow H\nu_e\bar{\nu}_e$ with respect to $e^+e^- \rightarrow He^+e^-$. Also for this kind of signals, if the final state corresponds to two Z's decaying purely hadronically, one is in principle forced to consider CC and MIX processes together with them.

In the following we will consider only the semileptonic six fermion CC processes for the case in which there is no Higgs contribution. The full calculation will be used to discuss top top events in the continuum and WWZ events.

For what concerns top physics, after its discovery and the measurement of its mass ($m_t = 174 \pm 6$ GeV) [15], it is extremely important to determine its properties with high-precision. Just because of the very large mass, they are most likely affected by the Higgs particles, and the top will surely play a crucial role in any theory of flavour dynamics. An extremely important characteristic of the top is its lifetime, which is much shorter than the time scale of strong interactions, allowing to study it in the context of perturbative QCD. Even if a proper toponium resonance cannot be formed at such a high top mass, perturbative effects result in a sharp rise of the cross section at threshold [16], superimposed on the natural sharp rise due to the opening of a new channel. For such a reason, in order to measure top mass the best strategy is probably to have the future e^+e^- collider run at $t\bar{t}$ threshold, while its static properties, such as magnetic and electric dipole moments [17] will be measured with high accuracy in the continuum, at higher energies. Our results refer only to the continuum top top production. Our tree level matrix elements for the complete calculation of the various final states, cannot in fact take into account the above mentioned threshold corrections. They are nevertheless useful to understand at any energy the relevance of the *production* \times *decay* approximation on the various physical quantities to be measured. Also at threshold they can for instance be used to estimate the irreducible background due to all non double resonant diagrams.

Another reason why top top in the continuum has to be carefully computed is that it constitutes a severe background to WWZ events. These events are important on their own, as they allow to measure gauge couplings. In particular the quartic gauge coupling and its possible deviations from SM will be studied in this reaction at future e^+e^- colliders. Several studies [18, 19] have already analyzed three vector boson production and anomalous gauge couplings. Actually LHC measurements on VV+X (V=W,Z) final states will reach a better quartic gauge sensitivity than the WWZ measurement at 500 GeV e^+e^- colliders.[20, 19] Nevertheless the cleaner e^+e^- experimental environment as well as the possibility of achieving higher energies or luminosities require a careful theoretical study. We therefore consider all possible contributions to WWZ signal and backgrounds as they can be defined in the realistic six fermion final state. In particular we analyze the sum of all semileptonic channels with four quarks in which WWZ can decay. We sum over all final states not containing b quarks, so that b-tagging can help to reduce most of $t\bar{t}$ background.

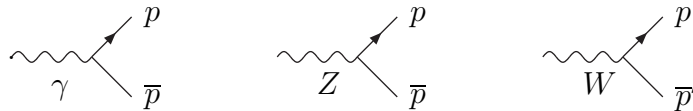
3 Six fermion processes calculation

Among the processes that our program SIXPHACT computes, one can distinguish CC209, CC418, CC836. As customary in four fermion physics, the numbers after CC refer to the Feynman diagrams of the process. Those we have indicated count diagrams without Higgs only. Examples of CC209 are $e^+e^- \rightarrow \mu\bar{\nu}_\mu u\bar{d}b\bar{b}$ and $e^+e^- \rightarrow \mu\bar{\nu}_\mu u\bar{d}s\bar{s}$. The number of Higgs diagrams for these processes is respectively 23 and 1. For processes with b's in the final state, we exactly account for the masses both in the matrix elements and in the phase space. Apart from the masses and couplings, all processes of this kind have the same matrix elements. The CC418 processes can be obtained from the previous ones with the exchange of two identical fermions in the final state or with the exchange of a fermion from the initial state with one from the final. So we can have two different types: CC418_f for processes like $e^+e^- \rightarrow \mu\bar{\nu}_\mu u\bar{d}u\bar{u}$ or $e^+e^- \rightarrow \mu\bar{\nu}_\mu u\bar{d}d\bar{d}$ and CC418_i for the ones of the type $e^+e^- \rightarrow e^-\bar{\nu}_e u\bar{d}s\bar{s}$. Analogously, CC836 are obtained by CC209 with two exchanges, one between initial and final and the other between two final particles, as it happens for $e^+e^- \rightarrow e^-\bar{\nu}_e u\bar{d}u\bar{u}$. There are processes which can have more exchanges, like $e^+e^- \rightarrow e^-\bar{\nu}_e u\bar{d}e^-e^+$ (CC1248). These are however of no interest for top physics and have a very low cross section as compared to the sum of four quarks CC final states, and we will not consider them.

The complexity of the problem is not only due to the great number of rather complex diagrams: the integration on the phase space is at least thirteen dimensional, but it becomes seventeen dimensional for the more realistic case in which initial state radiation (ISR) and beamstrahlung (BST) are accounted for. For such reasons it is extremely important to use a method for computing helicity amplitudes which allows a very fast and precise computation. We have used to this end PHACT [21], a set of routines based on the method of ref.[3], in order to generate the fortran code for the amplitudes. The resulting program SIXPHACT is able to compute the cross sections in reasonable cpu time (of the order of a few hours on a alphastation) with such a precision as to allow at the same time to generate differential cross sections (distributions) without visible statistical fluctuations. This normally requires a precision of the order of at least .5% on every bin and an overall precision at least ten times better.

As far as the matrix elements are concerned, we have computed all Feynman diagrams by calculating parts of diagrams of increasing complexity. The method used is particularly suited for this procedure and we will briefly explain it.

We start with the subdiagrams corresponding to a γ , a Z or a W into a pair of external fermions:



and then we compute the sum of subdiagrams defined in eqs. 1-8. Here and in the following, we use the prime to indicate a particle associated in an weak isospin doublet. So if, for instance, p will represent an up quark, \bar{p}' will indicate an anti-down quark. We will also use the symbols p, q, P to indicate external momenta, while r, s will

correspond to momenta which might be both external or internal. Eq. (1) represents the sum of γ and Z insertions of the subdiagrams above in a fermion line:

$$\begin{array}{c} r \\ | \\ \text{---} \gamma Z \text{---} \\ | \\ s \end{array} \begin{array}{c} p \\ / \\ \bar{p} \end{array} = \begin{array}{c} r \\ | \\ \text{---} \gamma \text{---} \\ | \\ s \end{array} \begin{array}{c} p \\ / \\ \bar{p} \end{array} + \begin{array}{c} r \\ | \\ \text{---} Z \text{---} \\ | \\ s \end{array} \begin{array}{c} p \\ / \\ \bar{p} \end{array} \quad (1)$$

The diagrams of eq. (2) correspond to a virtual W "decaying" into four outgoing fermions:

$$\begin{array}{c} \text{---} W \text{---} \end{array} \begin{array}{c} p \ \bar{p}' \\ q \ \bar{q} \end{array} = \begin{array}{c} p \\ / \\ \text{---} \gamma Z \text{---} \\ / \\ \bar{q} \end{array} \begin{array}{c} q \\ / \\ \bar{q} \end{array} + \begin{array}{c} p \\ / \\ \text{---} \gamma Z \text{---} \\ / \\ \bar{q} \end{array} \begin{array}{c} q \\ / \\ \bar{q} \end{array} \\
 + \begin{array}{c} q \\ / \\ \text{---} W \text{---} \\ / \\ \bar{p}' \end{array} \begin{array}{c} p \\ / \\ \bar{p}' \end{array} + \begin{array}{c} p \\ / \\ \text{---} W \text{---} \\ / \\ \bar{p}' \end{array} \begin{array}{c} q \\ / \\ \bar{q} \end{array} \quad (2)$$

Notice that the third subdiagram refers to the cases of an external incoming $W^-(W^+)$ and up(down) type flavour for $q\bar{q}$. In the other cases, the internal W is not attached to q but to \bar{q} .

We do not compute the sums of diagrams of eq. (2) when q and \bar{q} correspond to incoming e^-e^+ . When a whole diagram is divided by a W propagator in two parts containing four fermions each, one may choose to compute one of the two as a subdiagram (2) and our choice is to compute the part not containing e^-e^+ .

The diagrams of eq. (3) correspond to a virtual γ (or Z) "decaying" into four outgoing fermions:

$$\begin{array}{c} \text{---} \gamma(Z) \text{---} \end{array} \begin{array}{c} p \ \bar{p}' \\ q \ \bar{q}' \end{array} = \begin{array}{c} p \\ / \\ \text{---} W \text{---} \\ / \\ \bar{q}' \end{array} \begin{array}{c} q \\ / \\ \bar{q}' \end{array} + \begin{array}{c} p \\ / \\ \text{---} W \text{---} \\ / \\ \bar{q}' \end{array} \begin{array}{c} q \\ / \\ \bar{q}' \end{array} + \dots$$

$$\text{Diagram 1} + \text{Diagram 2} + \text{Diagram 3} \quad (3)$$

The diagrams of Eq. (4) represent the sum of γ and Z insertions in a fermion line of the subdiagrams defined in eq. (3):

$$\text{Diagram 1} = \text{Diagram 2} + \text{Diagram 3} \quad (4)$$

The remaining subdiagrams to compute correspond to the emission of 4 fermions from the upper part of a fermion line. Let's start with the case in which the four fermions are all outgoing.

$$\text{Diagram 1} = \text{Diagram 2} + \text{Diagram 3} + \text{Diagram 4} \quad (5)$$

$$\text{Diagram 1} = \text{Diagram 2} + \text{Diagram 3} \quad (6)$$

When two of the emitted fermions are the incoming $e^+ e^-$, we use a different symbol and a somewhat different definition as the term with the "decay" of a virtual W , Z or γ into four fermions is missing:

$$\text{Diagram 1} = \text{Diagram 2} + \text{Diagram 3} \quad (7)$$

$$\begin{array}{c}
P \\
\downarrow \\
\text{---} \bigcirc \text{---} \\
\uparrow \\
e^- e^+
\end{array}
\begin{array}{c}
q \\
\nearrow \\
\gamma Z \\
\searrow \\
\bar{q}
\end{array}
=
\begin{array}{c}
P \\
\uparrow \\
\gamma Z \\
\downarrow \\
e^+ e^-
\end{array}
+
\begin{array}{c}
P \\
\uparrow \\
\gamma Z \\
\downarrow \\
e^- e^+
\end{array}
\begin{array}{c}
e^+ \\
\nearrow \\
\gamma Z \\
\searrow \\
q
\end{array}
\begin{array}{c}
\bar{q}
\end{array}
\quad (8)$$

With the previous definitions, having computed the appropriate subdiagrams, the 209 diagrams corresponding to the process $e^+e^- \rightarrow u \bar{d} \mu \bar{\nu}_\mu b \bar{b}$ reduce to the ones represented in fig. 1. The other amplitudes for CC418 and CC836 are then obtained from these ones just exchanging the momenta of the appropriate particles.

The phase space integration of these amplitudes requires particular care for different resonant structures of the various sets of diagrams. From a kinematical point of view a six particles phase space integration might be thought as a sequence of two-body decays into intermediate states that can be formed with whatever combination of external momenta. This sequence ends up into the physical outgoing particles. A set of integration variables is constituted by the invariant masses of the intermediate states and by the angular coordinates of the decay products in their rest frame. With a proper change of variable on some invariant masses we have smoothed out the resonant Breit-Wigner peaks. Different combinations of momenta have been evaluated for each subset of diagrams, in particular for what concerns the background contributions. We have essentially used three parametrizations. For the integration of diagrams of top signal we have used a $t\bar{t}W^+W^-$ resonant phase space. In it, we choose as integration variables the masses of the two tops and of the two W's, on which we perform the above mentioned change of variables. Analogously we have used a WWZ resonant phase space for off shell production of three vector bosons and a WW resonant one for top background. The numerical integration has been performed with Vegas [22].

The computations we present take into account both initial state radiation and beamstrahlung. ISR is introduced via the structure function method [23]. The integration with ISR is 15-dimensional. BST is introduced with a link to the program CIRCE [24]. This program generates distributions of the fractions x_1, x_2 of momenta carried by the incoming electron and positron after BST. Either one integrates over these distribution functions or one makes use of the unweighted generation by CIRCE of the above fractions. We have chosen this second possibility: for every integration point we generate with CIRCE a couple of x_1, x_2 and reconstruct the kinematics accordingly.

As far as QCD corrections are concerned, we have introduced them in the so called naive QCD approach (NQCD). This amounts to consider that we have diagrams with vertices which in narrow width approximation (NWA) correspond to *production* \times *decay* of W's, Z's, tops. In a fully extrapolated setup the corresponding correction for the decay is factorized and amounts to multiplying the W decay vertex by $(1+\alpha(m_W)/\pi)^{1/2}$,

the Z one by $(1 + \alpha(m_Z)/\pi)^{1/2}$ and the top one by

$$\left[1 - \frac{2\alpha_s(m_t)}{3\pi}f(y)\right]^{\frac{1}{2}}, \quad \text{with } y = \left(\frac{m_W}{m_t}\right)^2. \quad (9)$$

The function $f(x)$ has been calculated in ref.[25] and, in the m_b/m_t , $\Gamma_W/M_W \rightarrow 0$ limit, it can be written in the compact form:

$$f(y) = \frac{2\pi^2}{3} - \frac{5}{2} + 2 \ln(y) \ln(1-y) + 4Li_2(y) - 2y + \frac{1}{1+2y} \left[(5+4y) \ln(1-y) + \frac{2y \ln(y)}{1-y} - \frac{4y^3(1-y+\ln(y))}{(1-y)^2} \right] \quad (10)$$

As a result of the strong correction, the top width lowers by a factor of order 10%.

We have also included the QCD corrections in the naive formulation to the $t\bar{t}$ production vertices. The first order QCD corrections [26] to the on-shell top top production total cross section can be written as

$$\sigma = \sigma_{VV} \left(1 + \frac{4\alpha_s(m_t)}{3\pi}K_V\right) + \sigma_{AA} \left(1 + \frac{4\alpha_s(m_t)}{3\pi}K_A\right). \quad (11)$$

For the exact expressions of $K_{V,A}$ we refer to Ref.[26]. σ_{VV} and σ_{AA} are the contributions to the total cross section coming respectively from the pure vectorial part and the pure axial part of the top couplings to γ , Z . We have not applied any correction to the interference term σ_{VA} which vanishes when integrated over the full phase space. Our treatment of QCD corrections is in any case exact only in the narrow width approximation for the total cross section with no cuts. In all other cases it must be considered as a rough estimate of the most important QCD corrections. In many cases this has however proved to be a reasonable approximation, probably just because the error on the corrections reflects upon a much smaller error on the cross sections.

For the numerical part we have used the G_μ -scheme

$$s_w^2 = 1 - \frac{M_W^2}{M_Z^2}, \quad g^2 = 4\sqrt{2}G_\mu M_W^2 \quad (12)$$

and the input masses $m_Z = 91.1888$ GeV, $m_W = 80.23$ GeV. We have chosen $m_t = 180$ GeV and for m_b the running mass value $m_b = 2.7$ GeV. The top mass we have used is actually 1σ apart from the actual measured central value[15], but all our conclusions are of course insensitive to differences of the order of the experimental error in the top mass. For the strong corrections to Z, W and top decay widths and vertices we have used $\alpha_s(m_Z) = 0.123$ and evolved it to the appropriate scales.

We have moreover implemented the following general set of cuts :

- jet(quark) energy > 3 GeV;
- lepton energy > 1 GeV;

- jet-jet invariant mass > 10 GeV;
- lepton-beam angle $> 10^\circ$;
- jet-beam angle $> 5^\circ$;
- lepton-jet angle $> 5^\circ$.

Other cuts specific to particular studies will be described in the following.

Some results concerning top cross sections have been compared with computations performed by the Grace group[13] and we have found a substantial agreement.

4 Top in the continuum

The future e^+e^- colliders will produce a great number of top top events so that they can also be regarded as top factories: at 500 GeV the cross section $\sigma(t\bar{t})$ is of the order of .5 pb, which corresponds to about 10^4 events per year for an integrated luminosity of 20 fb^{-1} .

We consider now two specific final states: $e^+e^- \rightarrow \mu\bar{\nu}_\mu u\bar{d}b\bar{b}$ and $e^+e^- \rightarrow e\bar{\nu}_e u\bar{d}b\bar{b}$. We have computed at 500 GeV and at 800 GeV the cross sections due to the signal diagrams only, and the irreducible backgrounds due to all (207 for the μ and 416 for the e) other diagrams and their interference with the signal. The signal diagrams correspond to the first diagram of the second line of fig. 1 when in it only the first diagram of eq. (7) is used. The results are given in table 1

\sqrt{s} GeV	channel	$t\bar{t}$ signal (fb)	background (fb)
500	$\mu\bar{\nu}_\mu u\bar{d}b\bar{b}$	19.850(4)	0.736(3)
	$e\bar{\nu}_e u\bar{d}b\bar{b}$		0.778(5)
800	$\mu\bar{\nu}_\mu u\bar{d}b\bar{b}$	10.700(2)	1.007(4)
	$e\bar{\nu}_e u\bar{d}b\bar{b}$		1.21(2)

Table 1: Cross section for the processes $e^+e^- \rightarrow \mu\bar{\nu}_\mu u\bar{d}b\bar{b}$ and $e^+e^- \rightarrow e\bar{\nu}_e u\bar{d}b\bar{b}$.

Here and in the following we report between parenthesis the statistical integration errors on the last digit of the result. For instance 19.850(4) has to be intended as 19.850 ± 0.004 .

These values have been obtained taking into account b masses, the full set of diagrams, ISR, BST, NQCD corrections for the decay vertices of the W's, the Z, tops and also for $Z(\gamma)t\bar{t}$ vertex, as already explained.

Let us first discuss the relevance of these corrections on the specific example of $e^+e^- \rightarrow \mu\bar{\nu}_\mu u\bar{d}b\bar{b}$. In table 2 we report all results of this study.

$e^+e^- \rightarrow \mu\bar{\nu}u\bar{d}b\bar{b}$	$t\bar{t}$ signal (fb)	background (fb)
NWA	18.880(3)	0.848(3)
Born	18.286(3)	0.824(3)
ISR	17.419(3)	0.750(3)
ISR NQCD*	17.188(3)	0.753(3)
ISR NQCD* BST	17.303(3)	0.731(3)
ISR NQCD* SBAND	17.308(3)	0.728(3)
ISR NQCD* BST m_b	17.352(3)	0.736(3)
ISR NQCD BST m_b	19.850(4)	0.736(3)

Table 2: Cross section for the process $e^+e^- \rightarrow \mu\bar{\nu}u\bar{d}b\bar{b}$ at $\sqrt{s} = 500$ GeV for different sets of approximations

The first result (NWA) reproduces what one would obtain using on shell calculation of $t\bar{t}$ production with subsequent decays of the tops to bW and on shell decay of the W 's. Instead of computing it this way, we have used the fact that *production* \times *decay* results can be obtained as a limit of the corresponding off shell diagrams. One just performs the following substitution for unstable particles propagator denominators:

$$p^2 - m^2 + im\Gamma \quad \rightarrow \quad (p^2 - m^2 + im\gamma) \sqrt{\frac{\Gamma}{\gamma}} \quad (13)$$

and then let $\gamma \rightarrow 0$. We have performed such limit numerically: we have used $\gamma = 10^{-3}\Gamma$ and we have checked that the result does not vary diminishing γ .

The Born approximation signal result shows that taking into account the "off-shellness" of the unstable particles produces a non-negligible variation of some percent.

The introduction of ISR decreases the $t\bar{t}$ signal with respect to Born only. This is at first surprising as around 500 GeV $t\bar{t}$ Born cross section is decreasing with energy and ISR reduces the effective energy. In effect we will see in the following that beamstrahlung raises the cross section. We have also checked that at 800 GeV ISR also raises it. The point is that, as we have verified, at 500 GeV there is a probability of about 5% that ISR reduces the energy of the hard scattering below the $t\bar{t}$ threshold. This justifies the decrease, but it also points out that there is a relatively high probability that ISR takes the energy back around the threshold. For precision calculations the corrections at threshold should therefore be included also at 500 GeV.

In the subsequent results of table 2 we indicate with NQCD* the corrections to t 's, W 's and Z decay vertices, with NQCD these same corrections together with that of $Z(\gamma)t\bar{t}$ vertex. Introducing NQCD* lowers the signal. This fact can be easily understood if we compute the same variation in *production* \times *decay* approximation. The signal has two W 's decaying to $\mu\bar{\nu}$ and $u\bar{d}$ respectively. The result can be approximated by $t\bar{t}$ cross section multiplied by the two branching $\Gamma_{W \rightarrow \mu\bar{\nu}}/\Gamma_{Wtot}$ and $\Gamma_{W \rightarrow u\bar{d}}/\Gamma_{Wtot}$. Correcting

with NQCD* corresponds to multiplying each hadronic $\Gamma_{q\bar{q}'}$ by $1 + \alpha/\pi$. Γ_{Wtot} has therefore to be multiplied by $1 + 2\alpha/3\pi$. The two branchings (and hence approximately also the signal cross section) get in conclusion a factor $(1 + \alpha/\pi)/(1 + 2\alpha/3\pi)^2$ which explains the difference between ISR and ISR NQCD* entries.

Taking into account beamstrahlung (BST) results in a raise of the order of half per cent for the signal and of almost three per cent for the background. Of course such a variation can be energy and process dependent, exactly as it happens with ISR. The program CIRCE that we have used allows for different parametrizations of beamstrahlung effects. The one we have normally used is TESLA. We have tried also SBAND and from the result in table 2 one sees that it does not introduce sensible differences from TESLA.

The introduction of the (running) b mass produces only a few permill variation.

It has to be noticed an important contribution (more than 10%) to $\sigma(\text{signal})$ coming from the NQCD correction of the vertex $Z(\gamma)t\bar{t}$. It may of course be questionable the way we have introduced such a correction, but in view of its numerical relevance, we have considered that even a very crude approximation was better than neglecting it, especially in considerations of the relative importance of signal and background.

Having briefly discussed the various approximations, let us now come to the main point of considering the irreducible background due to all diagrams contributing to a final state. From table 1 one can conclude that the background is important as it represents a correction of about 4% to the signal. Nevertheless such a statement has to be analyzed in more detail with the help of figs. 2 - 4. In fig. 2 and 3 it is reported the invariant mass distribution of the top candidate in the channel $e^+e^- \rightarrow \mu\bar{\nu}u\bar{d}b\bar{b}$. We have not reported the similar figure for $e^+e^- \rightarrow e\bar{\nu}u\bar{d}b\bar{b}$ as the conclusions are practically identical. From table 1 one can easily see in fact that the difference between the two channels (μ and e) is sizeable with respect to the backgrounds themselves, but it amounts to only a few permill of the signal.

Given such a final state, one is faced with the problem of trying to identify the particles which might come from a top decay. In any single event one can try to measure the invariant mass of three particles which could form the top. Three of them are the muon, its neutrino and the \bar{b} . From this triplet it is experimentally difficult to reconstruct the invariant mass, because the neutrino momentum can be deduced only from missing momentum, to which also ISR and BST contribute. The best strategy is to try to identify the three quarks forming the top. We assume that there is b tagging, and we require that both b's are identified, so that they are separated from the other two quarks. One cannot distinguish between a b and a \bar{b} . The only possibility is to form two invariant masses with one of the two b's and the other light quarks. Considering the distribution on the sum of these two invariant masses, it will be possible to measure the mass of the top. Once this has been measured, one can look for the nearest to the expected top mass between the two invariant masses. We refer to this one as the mass of the top candidate, and we have plotted its distribution. In fig. 2 one can see the differences among this distribution, the one due to the signal diagrams and that due to background diagrams. Also this last distribution peaks at the top mass. This is of course due to the many diagrams which are "single resonant", in which one of the two

top propagators can go on mass shell. We have also computed the distribution after some cuts have been applied to partially eliminate the background (dotted lines). The cuts we have imposed are:

$$|m(\text{ud}) - m_W| < 20 \text{ GeV} \quad |m(b\bar{b}) - m_Z| > 20 \text{ GeV} \quad (14)$$

One can see that these cuts reduce in fact the background by about a factor two, but they do not affect the peak at the top mass.

In fig. 3 we have reported on a linear scale and on the neighborhood of the peak the three curves relative to full process, signal and full process after cuts, both at 500 GeV and at 800 GeV. From these curves one concludes that there doesn't seem to be any difference in the location of the maximum, but there are some appreciable differences in the height between signal and total distributions. The cuts (14) do not seem to help in this region.

We have also studied the angular dependence of the top candidate. This is reported in fig. 4. If one compares the dashed and full curves, one notice that both at 500 GeV and at 800 GeV, there is a difference in the angular distribution between signal and total calculations. This is particularly relevant in the forward e^+ direction. In order to try to reduce the contribution of the irreducible background, we have studied the total distribution with the cuts (14) and an additional cut on the mass of the top candidate m_{tc} :

$$|m_{tc} - m_t| < 40 \text{ GeV} \quad (15)$$

The net result of such cuts, as it can be seen from the dotted curves, is to effectively reduce the irreducible background in the forward direction, but a mild distortion of the total curve, with respect to the signal one, remains also after the cuts.

The study of possible cuts is of course not exhausted by this short discussion, and the distributions presented are just an example of how one can handle this problem with complete calculations.

5 WWZ and its background

In this section we study the semileptonic processes in which there are no b 's in the final state. As we have already mentioned in section 2, one of the reasons why these processes are of interest is that they allow to study WWZ formation and decay where it will be possible to test the quartic gauge coupling.

The diagrams one has to deal with are essentially those for the full calculations of the preceding section. The main difference comes from the fact that those diagrams which were double or single resonant for top propagators, now do not have the top or antitop as an intermediate state, but a lighter quark. Their contribution is therefore greatly reduced and the corresponding total cross section decreases by an amount comparable to the size of $t\bar{t}$ signal diagrams.

The most important contribution to the cross section for the processes at hand comes from the 15 diagrams which correspond to WWZ production and decay. These have three resonant vector boson propagators and we will call them signal diagrams. The remaining ones can be divided in double, single and non resonant parts.

The results we will present will take into account ISR, BST, NQCD. We want to point out that for these processes the difference between calculations taking or not into account beamstrahlung is important. In fact, if we take as an example the process $e^+e^- \rightarrow \mu\bar{\nu}_\mu u\bar{d}s\bar{s}$, the full cross section is .18480(9) fb without BST and .18033(9) fb with BST. That for WWZ signal only is .17739(3) fb without BST and .17303(3) fb with BST. So the difference is of the order of two percent. If we compare this with the analogous differences in the case of top signal (half percent) and top background (almost three percent), we realize once again that BST effects are process (and cuts) dependent. Similarly to what happens for ISR, one cannot just ignore or approximate them with an overall factor.

In table 3 we present the cross sections for the full processes, those computed taking into account signal diagrams only, and those computed via the *production* \times *decay* approximation. This last result can also be obtained taking the narrow width approximation limit of the signal diagrams. We have taken such a limit numerically as we have done for the top case.

process	WWZ NWA (fb)	WWZ signal (fb)	complete (fb)
$\mu\bar{\nu}u\bar{d}c\bar{c}$	0.13836(2)	0.13464(2)	0.16218(9)
$e\bar{\nu}u\bar{d}c\bar{c}$			0.1783(2)
$\mu\bar{\nu}u\bar{d}s\bar{s}$	0.17780(3)	0.17303(3)	0.1803(1)
$e\bar{\nu}u\bar{d}s\bar{s}$			0.2117(2)
$\mu\bar{\nu}u\bar{d}u\bar{u}$	0.12815(2)	0.12469(2)	0.1512(1)
$e\bar{\nu}u\bar{d}u\bar{u}$			0.1758(3)
$\mu\bar{\nu}u\bar{d}d\bar{d}$	0.16468(3)	0.16025(3)	0.16733(9)
$e\bar{\nu}u\bar{d}d\bar{d}$			0.1941(1)

Table 3: Cross section for the processes $e^+e^- \rightarrow l\bar{\nu}_l + 4$ light quarks ($l = \mu, e$) at $\sqrt{s} = 500$ GeV

The difference between the full calculation and on shell (NWA) approximation is indeed remarkable. Even finite width effects are of some importance as they determine a variation of some percent between signal and NWA. We notice that the background is much higher in a process with an up-type quark pair than in the analogous one with down-type. For instance $\mu\bar{\nu}u\bar{d}c\bar{c}$ background is .0275fb while the $\mu\bar{\nu}u\bar{d}s\bar{s}$ is .0073fb. As the dominant contributions to background are the double resonant ones, the previous consideration shows that for the set of cuts we are using, most background comes from diagrams with two resonant W's and a γ converting in a quark-antiquark pair. Diagrams with one resonant W and the pair coming from Z decay would in fact produce an opposite behaviour and the numerical difference between the two backgrounds approximately corresponds to that due to the different quark charges in $WW\gamma^*$ diagrams.

In presence of such big irreducible background, it is necessary to introduce other

cuts in order to try to isolate WWZ production. We have performed detailed studies of possible cuts and we present them in figs. (5-7). Obviously they are at parton level, but just this fact helps in understanding the theoretical differences and the size of the errors associated with the various approximations. In practice, before considering hadronization, detector simulations and so on, it is important to study whether the full calculation is needed for a certain set of cuts or, for instance, signal diagrams represent a viable approximation. This may indeed be understood performing a comparison at parton level.

We have implemented different cuts on invariant masses of the pairs of particles which should come from vector bosons, and computed the cross sections for the various cuts with the full set of diagrams, with only the fifteen signal diagrams, and with *production* \times *decay* or narrow width approximation. It is obvious that the cross sections computed with the last approximation are not sensible to such kind of cuts, as the vector bosons are always considered on shell. In figs. (5-8) the dotted lines refer to this case. For the above reason they are just straight lines and they are reported just as a reference to show where the on shell cross section lies. The other two kinds of lines represent signal (dashed) and complete (continuous) cross sections as a function of cuts.

In order to reduce the contribution of non WWZ diagrams (the so called irreducible background), one would like to constrain the invariant masses formed by the appropriate final particles to be as near as possible to those of two W's and a Z. The momentum of the neutrino is not directly measurable, and therefore the neutrino lepton invariant mass is difficult to measure. For this reason we first consider some cuts which act only on the quarks. We intend somehow to force two quarks to reproduce a W and the other two to reproduce a Z. As the four quarks are practically indistinguishable, we compute the invariant mass of any pair of quarks. We then accept an event if out of the three couples of pairs of quarks, one at least has a pair whose invariant mass is around M_W and the other pair around M_Z . In figs. 5-6 are reported the cross sections for such kind of cuts as a function of M_{cut} , which represents the size of the window around M_W and M_Z in which events are accepted: the quarks are required to form at least one couple of pairs whose invariant masses m_i ($i = 1, 2$) satisfy the conditions $|M_V - m_i| < M_{cut}$ ($V = W, Z$). Some comments are in order. Both figures show that the signal contribution to the cross section (dashed line) is lower than the NWA even for very loose cuts or for the cross section without cuts (see table 3). This implies that one cannot rely on the narrow width approximation. The fact that the full calculation at high M_{cut} approaches the NWA for the $\mu\bar{\nu}u\bar{d}s\bar{s}$ case (fig. 5) is probably just casual. It does not happen for $e\bar{\nu}u\bar{d}s\bar{s}$. The curves of fig. 6 show that for the electron case the difference between signal and total process is extremely relevant. It grows with the energy and the cuts we have imposed can greatly reduce the difference but not suppress it. For the muon case an M_{cut} of about 10 GeV is on the contrary sufficient to make total and signal cross section practically coincide. The loss in event number is however of the order of ten percent.

As we are interested primarily in WWZ physics, it is important to find out whether further cuts may allow also in the electron case to further suppress the background. We have therefore studied the possibility of imposing a cut also on the invariant mass

formed by the electron and the neutrino. In fig. 7 the cross sections for two cases are reported:

- a) quarks are required to form two pairs whose invariant masses m_i ($i = 1, 2$) satisfy the conditions $|M_V - m_i| < 15 \text{ GeV}$, $V = W, Z$ and $e^- \bar{\nu}_e$ are required to form an invariant mass m such that $|M_W - m| < M_{cut}$.
- b) quarks are required to form two pairs whose invariant masses m_i ($i = 1, 2$) satisfy the conditions $|M_V - m_i| < M_{cut}$, $V = W, Z$ and $e^- \bar{\nu}_e$ are required to form an invariant mass m such that $|M_W - m| < M_{cut}$.

In the latter case the simultaneous variation of M_{cut} is studied, while in the first we explore the possibility of having different cuts on the leptonic and quark system. As explained before the determination of νe invariant mass is affected by great experimental errors. For such a reason in fig. 7 we have reported the cross sections for this invariant mass and for the more realistic case in which the cut is imposed on the invariant mass formed with electron and reconstructed neutrino four momenta. We assign in the latter case all missing three-momentum \bar{p}_{mis} to the neutrino and take its energy to be equal to $|\bar{p}_{mis}|$.

The conclusions that can be drawn from fig. 7 are almost self evident: Comparing fig. 6 with fig. 7, one can verify that even introducing a very loose cut as $M_{cut}=60 \text{ GeV}$ on $e^- \bar{\nu}_e$ invariant mass reduces significantly the difference between signal and total cross sections. This means that the contribution of exchanged diagrams which were responsible of the great difference between the electron and the muon case is sensitive to this kind of cut. On the other hand, fig. 7 shows that if the cuts have to be so stringent to reduce the difference between signal and total cross section to the order of the percent, one loses more than one third of the event number, as compared to the NWA. This conclusion is important in view of the fact that such WWZ processes have a low cross section: at 500 GeV $\sigma(\text{WWZ})$ is of the order of 40fb, which corresponds to a total of 800 events per year for an integrated luminosity of 20 fb⁻¹.

The reactions we have just examined in figs. 5-7 have been used as a case study for the cuts, but in reality they cannot be directly measured. This is due to the fact that quark flavors cannot be disentangled experimentally. We examine therefore in fig. 8 the more interesting physical case in which we sum over all reactions involving μ 's. To this end we have computed for all different cuts the cross sections of the four reactions:

$$e^+ e^- \rightarrow \mu^- \bar{\nu}_\mu u \bar{d} s \bar{s} \quad e^+ e^- \rightarrow \mu^- \bar{\nu}_\mu u \bar{d} c \bar{c} \quad e^+ e^- \rightarrow \mu^- \bar{\nu}_\mu u \bar{d} u \bar{u} \quad e^+ e^- \rightarrow \mu^- \bar{\nu}_\mu u \bar{d} d \bar{d}$$

In the plot it is reported, both for WWZ diagrams and for the complete calculation, the sum of these cross sections multiplied by a factor 4. This accounts for the reactions in which one has $\mu^+ \nu_\mu \bar{u} d$ instead of $\mu^- \bar{\nu}_\mu u \bar{d}$ and for those in which one has $c \bar{s}$ (or $\bar{c} s$) instead of $u \bar{d}$ (or $\bar{u} d$). Under this exchanges the sum of the four reactions above remains the same for the present set of cuts. The dashed and continuous lines of fig. 8 give therefore the exact cross section (at order α^6) as a function of M_{cut} for all processes with one muon, four quarks and no b's in the final state.

We are implicitly assuming in these considerations that, in order to exclude the overwhelming background from $t \bar{t}$ production and decay, b-tagging will be used to

exclude all events with at least one tagged b . This is the reason why we do not sum on WWZ events with b 's in the final state. With actual b -tagging techniques, there is a high probability $P_{c \rightarrow b}$ (say of the order of thirty per cent) that a c be misidentified as a b . To take this into consideration, one should multiply by the appropriate reduction factors $1 - P_{c \rightarrow b}$, $(1 - P_{c \rightarrow b})^2$, $(1 - P_{c \rightarrow b})^3$ the contributions with one, two or three c 's to the the sums reported in fig. 8. This would lead to a decrease of the curves of about 25% for $P_{c \rightarrow b} = .3$.

True events with two b 's in the final state, which are dominated by top top signal can be misidentified and become an important background to WWZ physics as there is a finite probability $P_{b \nrightarrow b} = 1 - P_{b \rightarrow b}$ that a b may not be recognized as such. We have computed such a background as a function of M_{cut} . The chain dash and chain dot curves of fig. 8 correspond to the contribution of top top signal and background (to $t\bar{t}$ events) respectively. We have here assumed $P_{b \nrightarrow b} = .2$ and summed over the processes

$$e^+e^- \rightarrow \mu^- \bar{\nu}_\mu u \bar{d} b \bar{b} \quad e^+e^- \rightarrow \mu^- \bar{\nu}_\mu c \bar{s} b \bar{b} \quad e^+e^- \rightarrow \mu^+ \nu_\mu \bar{u} d b \bar{b} \quad e^+e^- \rightarrow \mu^+ \nu_\mu \bar{c} s b \bar{b}.$$

The first consideration on this background coming from top top events is that even an imperfect b tagging is of considerable help in strongly reducing the great number of these events. It has to be remarked that this background depends strongly on the applied M_{cut} . If one adopts the strategy of applying a severe M_{cut} of the order of 10 GeV, it is reduced to about 1/6 of WWZ signal. If on the other hand a milder M_{cut} is used or if $P_{b \nrightarrow b}$ is greater than what we used, it may become comparable to the signal itself. In such a case, other cuts may still be used. For instance we have verified that by requiring all four possible three jets invariant masses to be out of a window of 40 GeV around the top mass, one reduces the contribution of top top events to be less than that of the other diagrams for $b\bar{b}$ final states (chaindot curve in fig. 8), without sensible loss of WWZ signal.

6 Conclusions

We have computed tree level semileptonic six fermion processes which will become relevant for the future e^+e^- linear colliders. Our results concern at present the infinite Higgs mass limit. The helicity amplitude method used [21][3] has allowed us to build up a program (SIXPHACT) which is able to produce technically precise results in reasonable computer time. This was far from obvious at the start, given the complexity of treating a 6 body final state and the great number of complex Feynman diagrams. Speed and precision are essential to produce very reliable differential cross sections. These allow to exploit the true potentiality of six fermion complete calculations: it is just studying distributions that one can understand the differences from the usual *production* \times *decay* approximation and which cuts have to be imposed to enhance signals with respect to irreducible background.

The main drawback when dealing with complete tree level matrix elements is how to account for radiative corrections. In this respect on shell computations folded with decays are in a much better shape. On the other hand they completely lack the contributions to the physical final states of a large class of diagrams and they miss finite

width and spin correlation effects. In our opinion the two ways of approaching the physical problem are somehow complementary and must both be pursued. We have included initial state radiation and beamstrahlung. QCD corrections are taken into account in a simplified (naive) way, exact only in NWA for total cross sections without cuts.

We have given some examples of phenomenological studies relevant to top and WWZ physics at 500 and 800 GeV. We have in particular found that single resonant background contributions are difficult to get rid of when studying invariant mass or angular top distributions. For WWZ it seems that *production* \times *decay* approximation is not viable, and that to get rid of the irreducible background with the cuts we have tried, one loses about 10% of events with a muon in the final state and more than 30% for an electron at 500 GeV. The enormous amount of background coming from $t\bar{t}$ production seems to be completely disposed of with appropriate b-tagging and cuts. The effect of cuts does not influence the signal, while spurious b-tagging of signal events may result in a decrease of the order of 25%.

Acknowledgments

We wish to thank Yoshimasa Kurihara and Roberto Pittau for useful discussions. Comparisons with Y. Kurihara and F. Yuasa are also gratefully acknowledged.

References

- [1] M.Jacob, J.C. Wick, *Ann. Phys.* 7 (1959) 404;
J.D. Bjorken, M.C. Chen, *Phys. Rev.* 154 (1966) 1335;
O. Reading-Henry *Phys. Rev.* 154 (1967) 1534;
- [2] P. De Causmaecker, R. Gastmans, W. Troosts, T. T. Wu, pl B105 1981 215, *Nucl. Phys.* B206 (1982) 53;
F.A. Berends, R. Kleiss, P. De Causmaecker, R. Gastmans, W. Troosts, T. T. Wu, *Nucl. Phys.* B206 (1982) 61, B239 (1984) 382, B239 (1984) 395, B264 (1986) 243, B264 (1986) 265;
M. Caffo, E. Remiddi, *Helv. Phys. Acta.* 55 (1982) 3 39;
G.R. Farrar, F. Neri, *Phys. Lett.* B130 (1983) 109;
G. Passarino, *Phys. Rev.* D28 (1983) 2867, *Nucl. Phys.* B237 (1984) 249
F.A. Berends, P.H. Daverveldt, R. Kleiss *Nucl. Phys.* B253 (1985) 441;
R. Kleiss, W.J. Stirling, *Nucl. Phys.* B262 (1985) 235, *Phys. Lett.* B179 (1986) 159;
J. Gunion, Z. Kunszt, *Phys. Lett.* B161 (1985) 333;
K. Hagiwara, D. Zeppenfeld, *Nucl. Phys.* B274 (1986) 1;
Z. Xu, Da-Hua Zhang, L. Chang *Nucl. Phys.* B291 (1987) 392.
- [3] A. Ballestrero, E. Maina, *Phys. Lett.* B350 (1995) 225.
- [4] T. Sjöstrand, *Comp. Phys. Commun.* 82 (1994) 74;
G. J. van Oldenborgh, P. J. Franzini, A. Borrelli,

- Comp. Phys. Commun.* 83 (1994) 14;
 F.A. Berends, R. Pittau, R. Kleiss, *Comp. Phys. Commun.* 85 (1995) 437;
 M. Skrzypek, S. Jadach, W. Placzek, Z. Was, prep. CERN-TH-95-205 (1995);
 F. Caravaglios, M. Moretti, *Phys. Lett.* B358 (1995) 332;
 G. Passarino, *Comp. Phys. Commun.* 97 (1996) 261;
 H. Anlauf, P. Manakos, T. Ohl, H. D. Dahmen, prep. IKDA-96-15 (1996), hep-ph/9605457;
 D. Bardin et al., prep. DESY-96-233 (1996), hep-ph/9612409;
 D. G. Charlton, G. Montagna, O. Nicrosini, F. Piccinini, *Comp. Phys. Commun.* 99 (1997) 355;
 C. G. Papadopoulos, *Comp. Phys. Commun.* 101 (1997) 183;
 J. Fujimoto et al., *Comp. Phys. Commun.* 100 (1997) 128;
 P.A. Baikov et al., prep. HEP-9701412 (1997), hep-ph/9701412.
- [5] E. Accomando, A. Ballestrero, *Comp. Phys. Commun.* 99 (1997) 270.
- [6] Physics at LEP2, G. Altarelli T. Sjostrand, F. Zwirner eds., CERN 96-01
- [7] D. Bardin, R. Kleiss et al., *Event Generators for WW Physics* in ref. [6]
- [8] M. L. Mangano, G. Ridolfi et al., *Event Generators for Discovery Physics* in ref. [6]
- [9] F.A. Berends, P.H. Daverveldt, R. Kleiss, *Nucl.Phys.* B253(1985)441;
 D. Bardin, M. Bilenky, A. Olchevski, T. Riemann,
Phys. Lett. B308(1993)403; E:[ibid.B357(1995)725];
 T. Ishikawa, T. Kaneko, S. Kawabata, Y. Kurihara, Y. Shimizu, H. Tanaka,
 prep. KEK-92-210 (1993);
 F.A. Berends, R. Kleiss, R. Pittau, *Nucl.Phys.* B424(1994)308;
Nucl.Phys. B426(1994)344; *Nucl.Phys. B, Proc. Suppl.* 37B(1994)163;
 Y. Kurihara, D. Perret-Gallix, Y. Shimizu, *Phys. Lett.* B349(1995)367;
 G. Montagna, O. Nicrosini, G. Passarino, F. Piccinini, *Phys. Lett.* B348(1995)178;
 C. G. Papadopoulos, *Phys. Lett.* B352(1995)144;
 D. Bardin, T. Riemann, *Nucl. Phys.* B462(1996)3;
 F. Caravaglios, M. Moretti Oxford prep. OUTP-96-13-P, Apr 1996;
 E. Accomando, A. Ballestrero, G. Passarino, *Nucl. Phys.* B476 (1996) 3.
- [10] E. Boos, M. Sachwitz, H.J. Schreiber, S. Shichanin, *Z. Phys.* C61 (1994) 675;
Z. Phys. C64 (1994) 391; *Int. J. Mod. Phys. A*10 1995 2067;
Z. Phys. C67 (1995) 613;
 M. Dubinin, V. Edneral, Y. Kurihara, Y. Shimizu, *Phys. Lett.* B329 (1994) 379;
 D. Bardin, A. Leike, T. Riemann, *Phys. Lett.* B344 (1995) 383;
Phys. Lett. B353 (1995) 513;
 D. Apostolakis, P. Ditsas, S. Katsanevas, prep. CRETE-96-12 (1996), hep-ph/9603383;
 G. Montagna, O. Nicrosini, F. Piccinini, *Phys. Lett.* B348 (1995) 496;
 G. Passarino, *Nucl. Phys.* B488 (1997) 3.

- [11] A. Ballestrero, E. Maina, S. Moretti, *Phys. Lett.* B333 (1994) 434
A. Ballestrero, E. Maina, S. Moretti, *Phys. Lett.* B335 (1994) 460.
- [12] G. Montagna, M. Moretti, O. Nicrosini, F. Piccinini Pavia Prep. FNT/T-97/10, hep-ph/9705333
- [13] Y. Kurihara and F. Yuasa, private communication.
- [14] D. Bardin, M. Bilenky, D. Lehner, A. Olchevski, T. Riemann, Nucl. Phys. (Proc. Suppl.) 37B (1994) 148;
- [15] F. Abe et al. (CDF Coll.), *Phys. Rev.* D50 (1994) 2966 and *Phys. Rev. Lett.* 74 (1995) 2626; S. Abachi et al (D0 Coll.), *Phys. Rev. Lett.* 74 (1995) 2632.
- [16] V.S. Fadin, V.A. Khoze, JETP Lett. 46 (1987) 525, Sov. J. Nucl. Phys. 48 (1988) 309;
M.J. Strassler, M.E. Peskin, *Phys. Rev.* D43 (1991) 1500;
M. Jezabek, J.H. Kühn, T. Teubner, *Z. Phys.* C56 (1992) 653;
Y. Sumino, K. Fujii, K. Hagiwara, M. Murayama, C.K. Ng, *Phys. Rev.* D47 ((1992)) 56;
M. Jezabek, J.H. Kühn *Phys. Lett.* B316 ((1993)) 360.
- [17] W. Bernreuther, O. Nachtmann, P. Overmann, T. Schröder, *Nucl. Phys.* B388 (1992) 53, B406 (1993) 516;
G. L. Kane, G. A. Ladinsky, C. P. Yuan, *Phys. Rev.* D45 (1991) 124.
- [18] J. Kalinowsky *Acta Phys.Polon.* B23 (1992) 1237;
G. Blanger, F. Boudjema, *Phys. Lett.* B288 (1992) 201;
F. Boudjema, LAPP prep. ENSLAPP-A-431-93 (1993), hep-ph/9308343.
- [19] A. Miyamoto, Kek prep 95-185 (1995).
- [20] A. Dobado, M.J. Herrero, J.R. Pelaez, E. Ruiz Morales, M.T. Urdiales, *Phys. Lett.* B352 (1995) 400;
A. Dobado, M.T. Urdiales, *Z. Phys.* C71 (1996) 659.
- [21] A. Ballestrero, PHACT 1.0 - Program for Helicity Amplitudes Calculations with Tau matrices; Torino prep. in preparation.
- [22] G.P. Lepage, *Jour. Comp. Phys.* 27 (1978) 192.
- [23] E. A. Kuraev, V. S. Fadin, Sov. J. Nucl. Phys. **41** (1985) 466;
G. Altarelli, G. Martinelli, in *Physics at LEP*, CERN Report 86-02, J. Ellis, R. Peccei eds. (CERN, Geneva 1986), vol I, pg. 47;
O. Nicrosini, L. Trentadue, *Phys. Lett.* B196 (1987) 551.
- [24] T. Ohl, prep. IKDA-96-13 (1996), hep-ph/9607454.
- [25] M. Jezabek, J.H. Kühn, *Nucl. Phys.* B314 (1989) 1, *Phys. Rev.* D48 (1993) 1910.

- [26] J. Jersak, E. Laermann, P.M. Zerwas, *Phys. Rev.* D25 (1982) 363; J. Schwinger, 'Particles, Sources and Fields', Addison-Wesley (1973); L. Reinders, H. Rubinstein, S. Yazaki, *Phys. Reports* C127 (1985) 1.

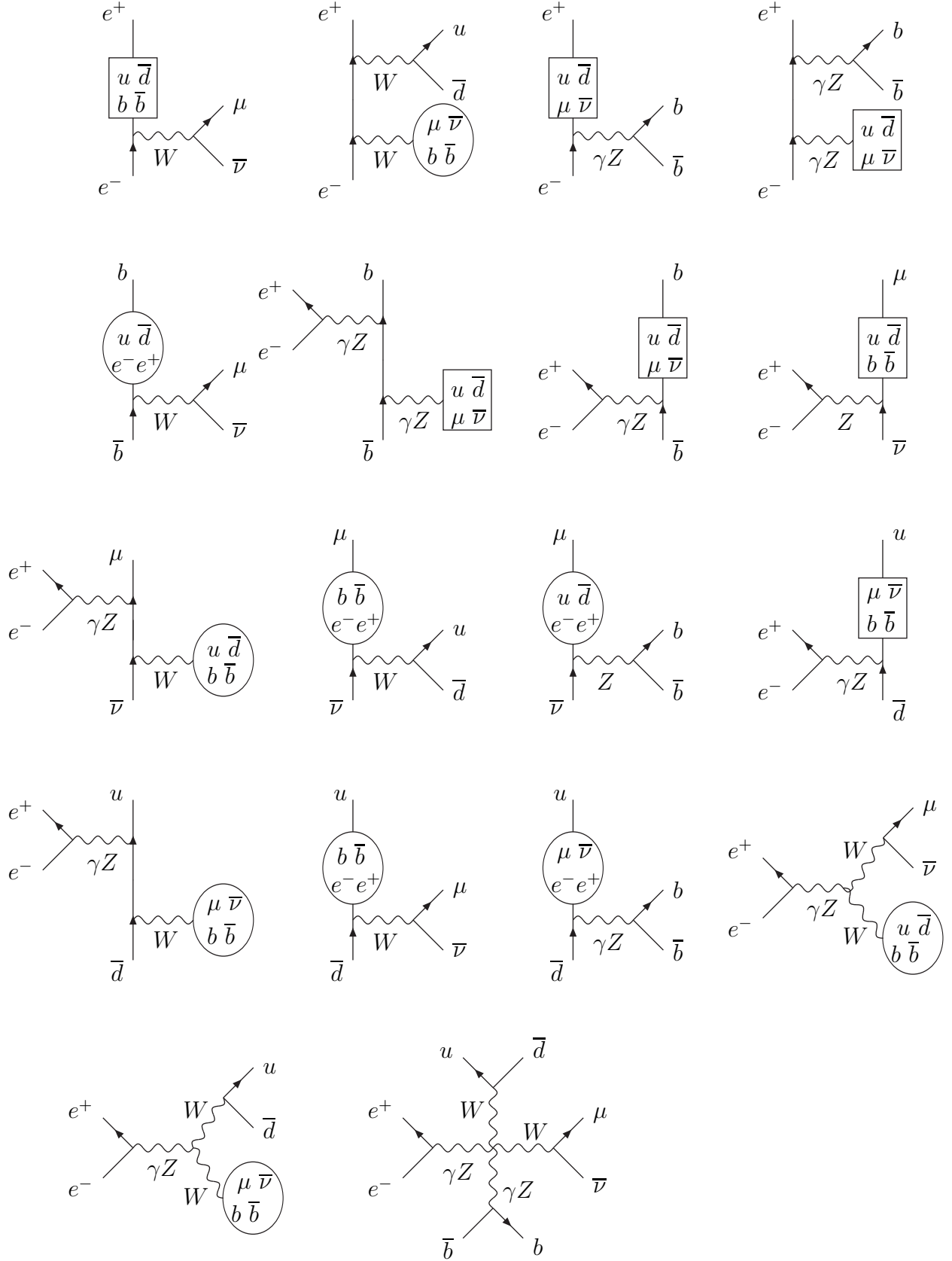


Figure 1: Diagrams for $e^+e^- \rightarrow u \bar{d} \mu \bar{\nu}_\mu b \bar{b}$

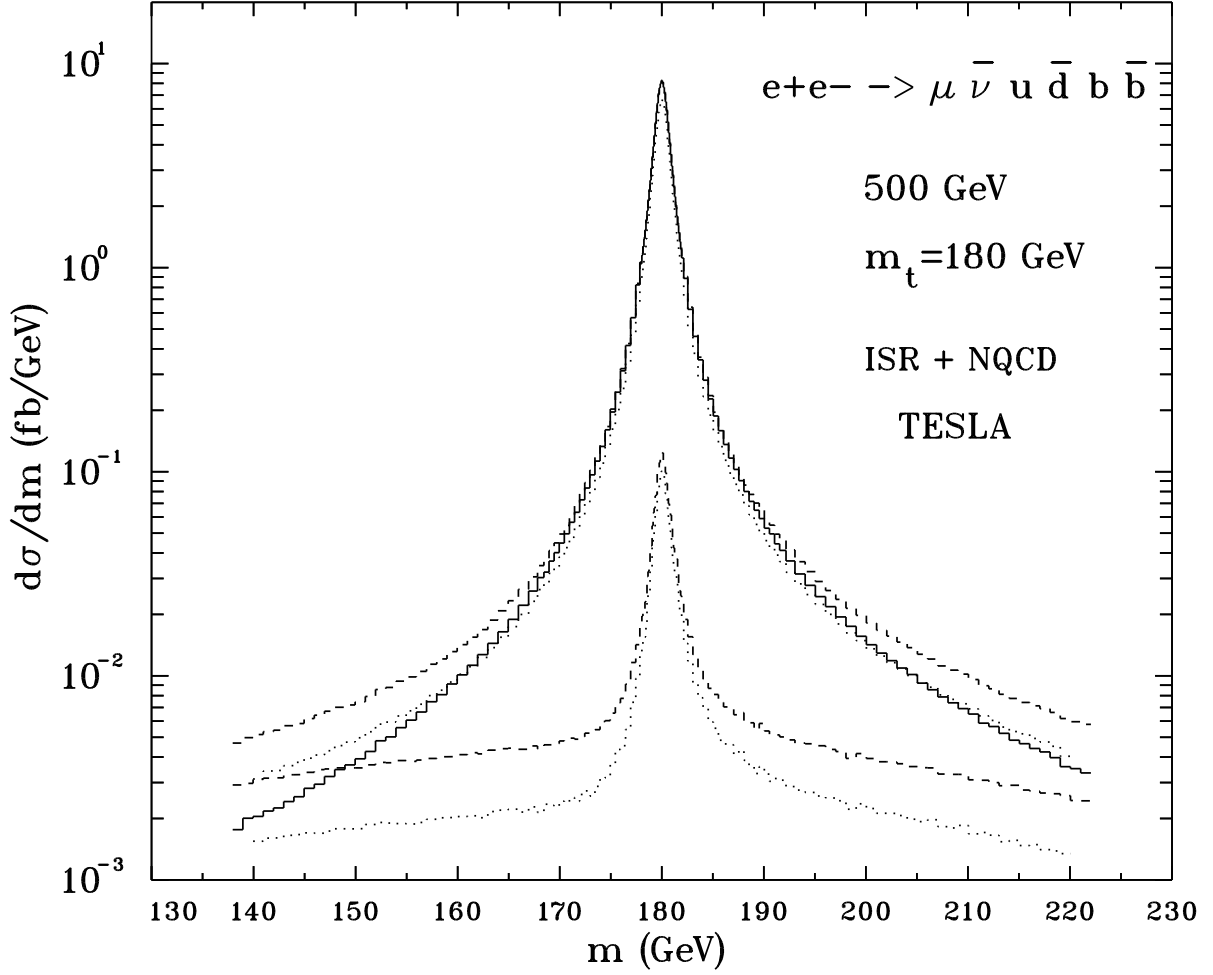


Figure 2: Invariant mass distribution for top candidate at $\sqrt{s} = 500$ GeV. The nearest to the nominal top mass between $u\bar{d}b$ or $u\bar{d}\bar{b}$ invariant masses is chosen event by event. The solid line represents the contribution of $t\bar{t}$ off shell signal. The dash lines represent the full process (upper) and the irreducible background (lower). The dot lines represent the full process (upper) and the irreducible background (lower) after cuts. Cuts are described in the text.

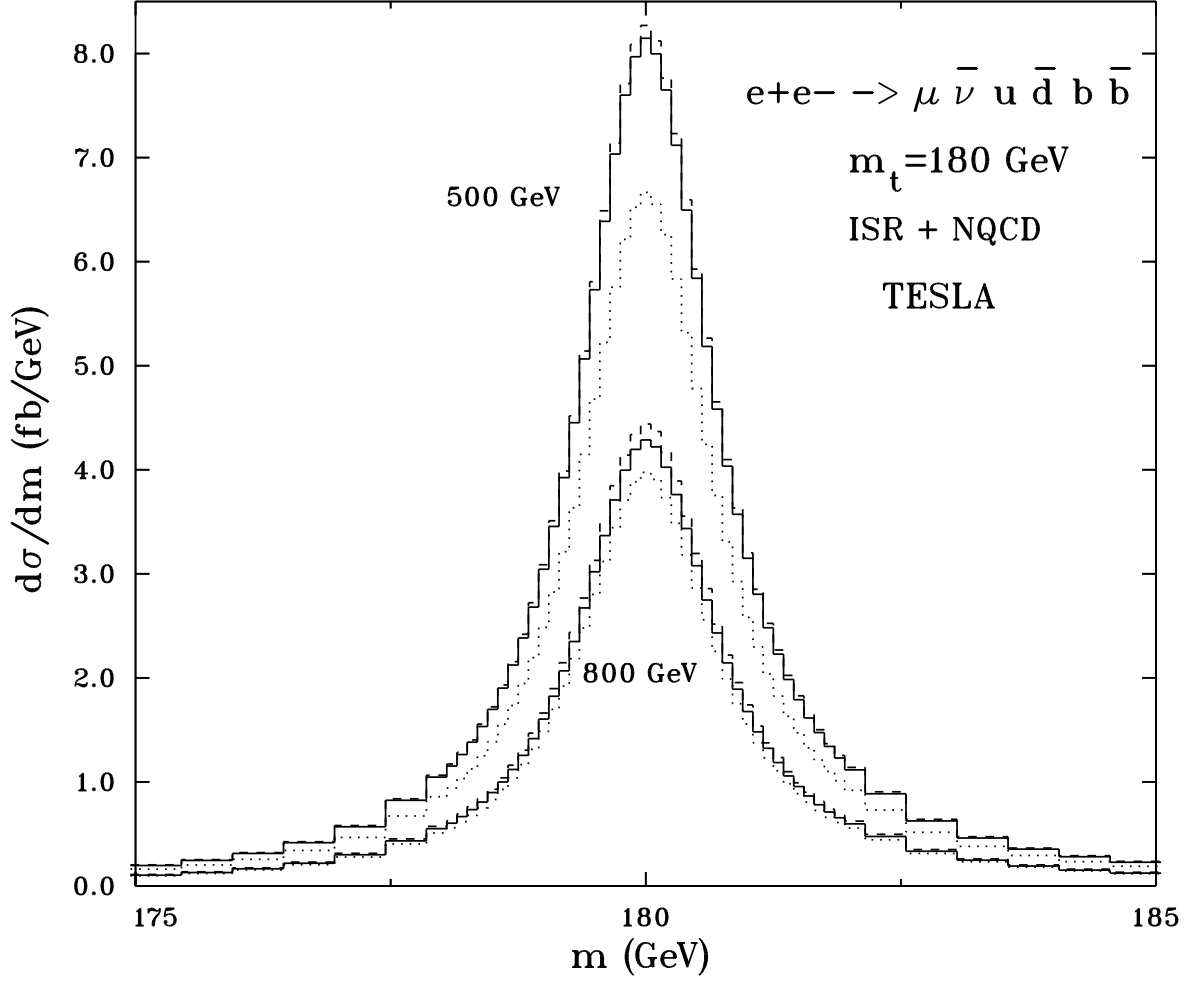


Figure 3: Invariant mass distributions for top candidate, detail of the peak zone on a linear scale at $\sqrt{s} = 500 \text{ GeV}$ (upper) and $\sqrt{s} = 800 \text{ GeV}$ (lower). The nearest to the nominal top mass between $u\bar{d}b$ or $u\bar{b}d$ invariant masses is chosen event by event. The solid lines represent the $t\bar{t}$ signal, the dash lines the full process while the dotted lines represent the full process after cuts. Cuts are described in the text.

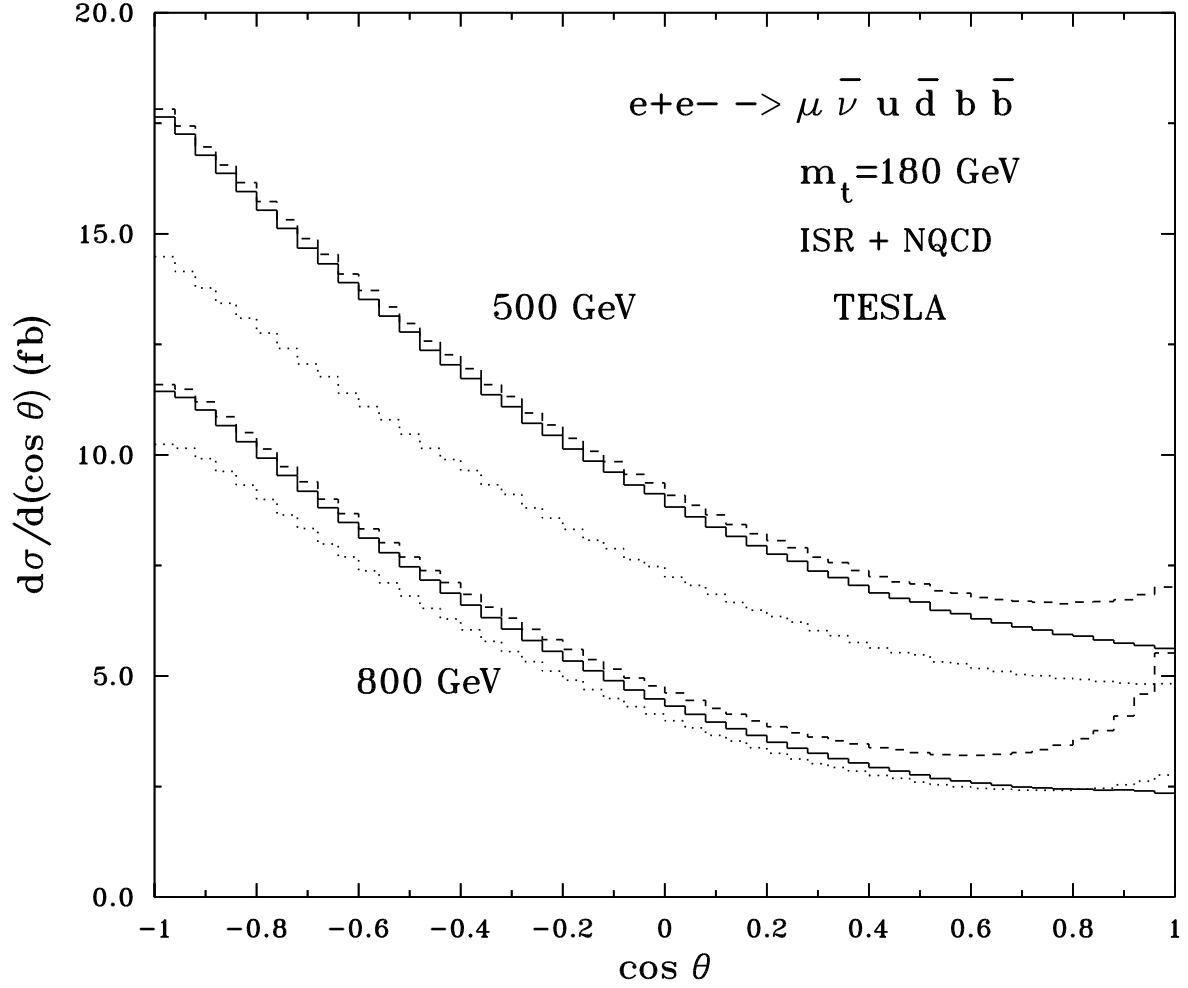


Figure 4: Angular distribution for top candidate at $\sqrt{s} = 500$ GeV (upper) and $\sqrt{s} = 800$ GeV (lower). The nearest to the nominal top mass between $u\bar{d}b$ or $u\bar{d}\bar{b}$ invariant masses is chosen event by event. The solid lines represent the contribution of $t\bar{t}$ off shell signal, the dash lines the full process and the dot lines the full process after cuts. Cuts are described in the text.

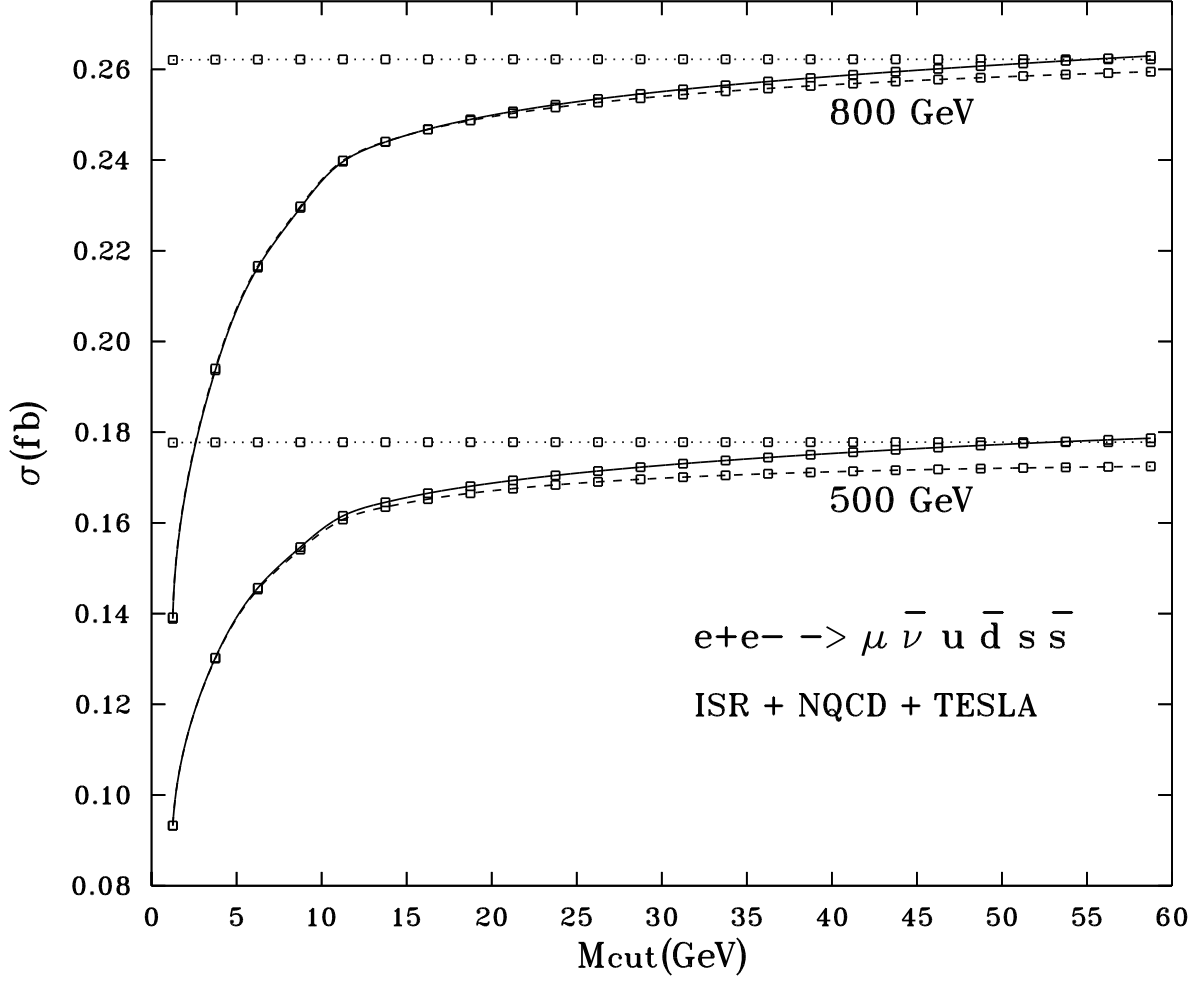


Figure 5: Cross section for the process $e^+e^- \rightarrow \mu\bar{\nu}_\mu u\bar{d}s\bar{s}$ as a function of M_{cut} at $\sqrt{s} = 500$ GeV (lower) and $\sqrt{s} = 800$ GeV (upper). Quarks are required to form two pairs whose invariant masses m_i ($i = 1, 2$) satisfy the conditions $|M_V - m_i| < M_{cut}$, $V = W, Z$. The dot lines represent the cross section due to WWZ on shell, the dashed ones the contribution of resonant WWZ diagrams only, the continuous the complete cross section. The markers indicate the points effectively computed.

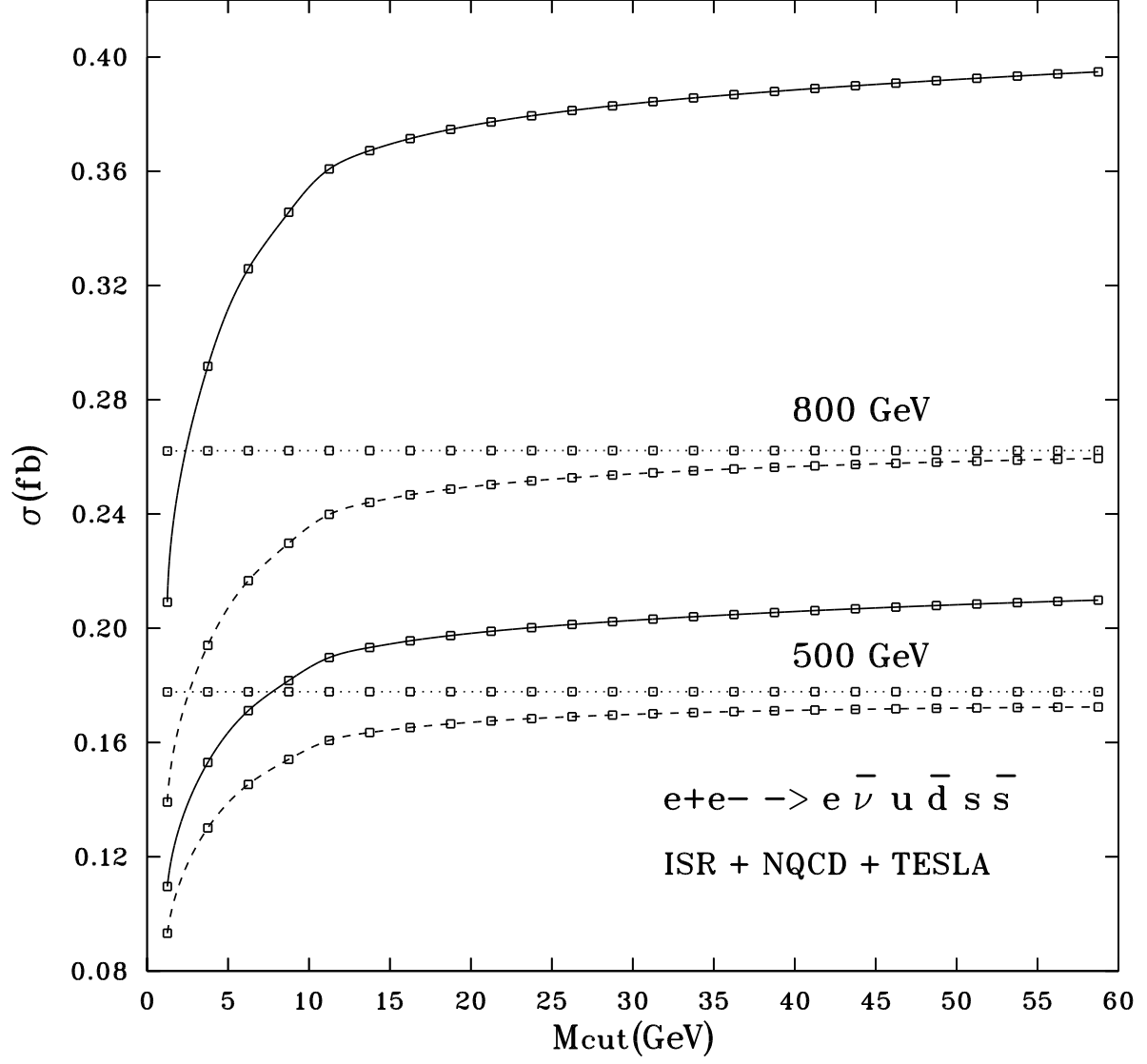


Figure 6: Cross section for the process $e^+e^- \rightarrow e^- \bar{\nu}_e u \bar{d} s \bar{s}$ at $\sqrt{s} = 500$ GeV (lower) and $\sqrt{s} = 800$ GeV (upper) as a function of M_{cut} . The definition of M_{cut} and the meaning of the different lines and of the markers is the same as in fig 5.

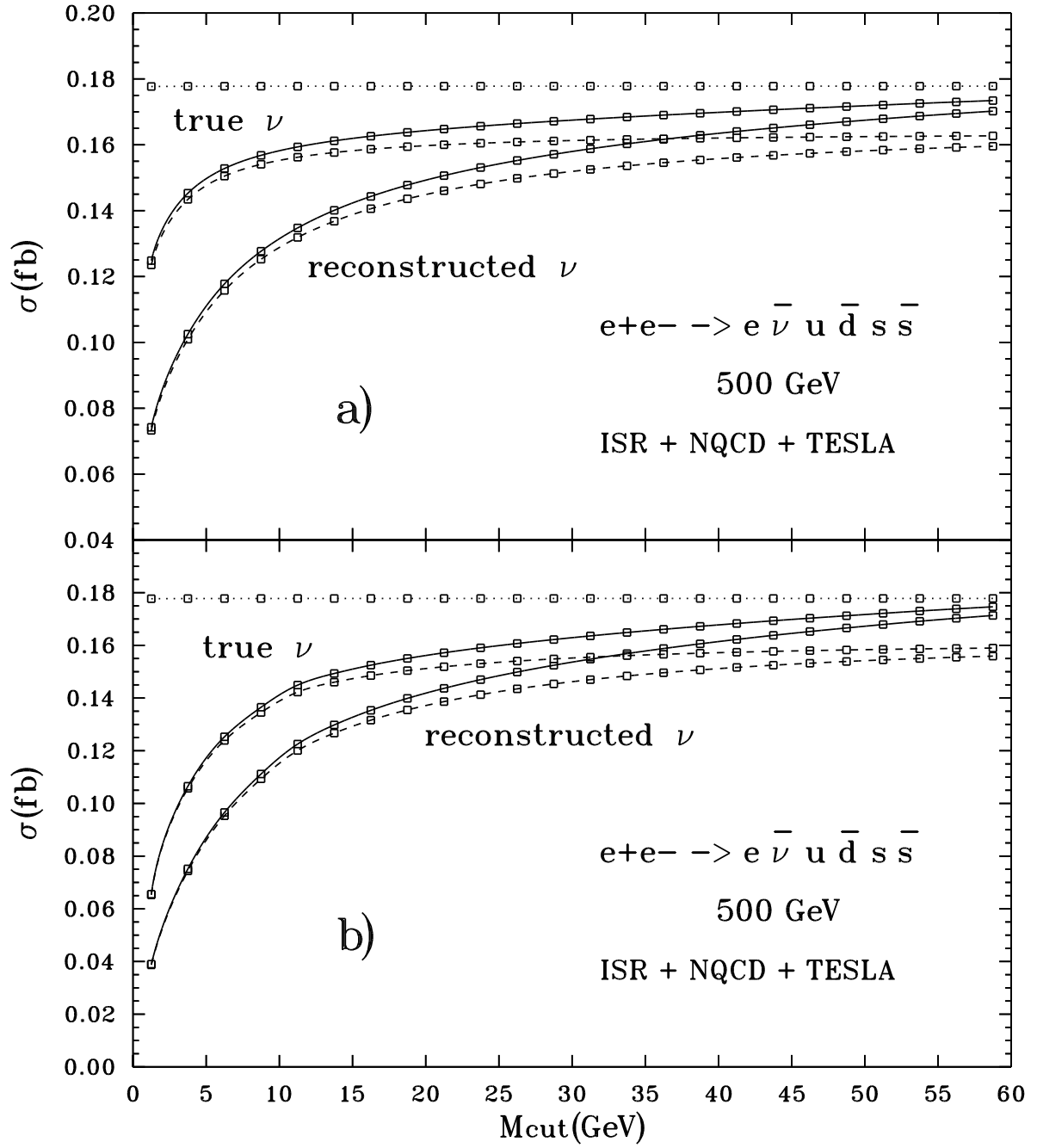


Figure 7: Cross section for the process $e^+e^- \rightarrow e^- \bar{\nu}_e u \bar{d} s \bar{s}$ at $\sqrt{s} = 500 \text{ GeV}$ as a function of M_{cut} . $e^- \bar{\nu}_e$ are required to form an invariant mass m such that $|M_W - m| < M_{\text{cut}}$. In case **a)** the quark cut defined in fig. 5 is kept fixed: $|M_V - m_i| < 15 \text{ GeV}$; in case **b)** it is varied together with the $e^- \bar{\nu}_e$ one. In each plot the two lower curves correspond to neutrino 3-momentum reconstructed from missing momentum. The definition of M_{cut} and the meaning of the different lines and of the markers is the same as in fig 5.

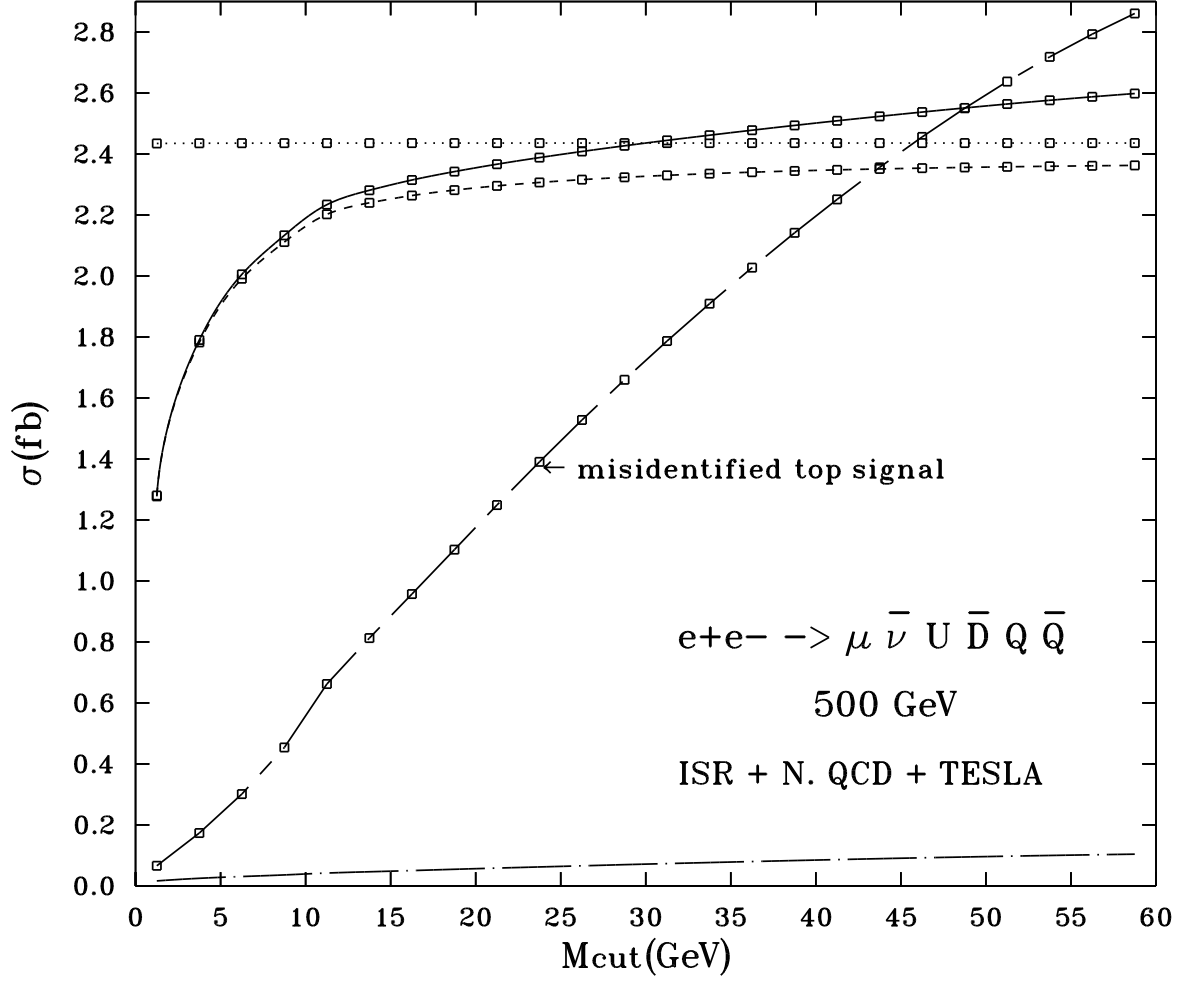


Figure 8: cross section for $e^+e^- \rightarrow \mu\nu U D \bar{Q} \bar{Q}$ as a function of M_{cut} . We sum over all processes with one muon and no b quarks. The chaindash (chaindot) line represents the background due to top top signal (background) with both misidentified b's. A 20% probability for each b quark to be misidentified is assumed. The definition of M_{cut} and the meaning of the different lines and of the markers is the same as in fig 5.